Physics Letters B 710 (2012) 426–429

Contents lists available at SciVerse ScienceDirect

Physics Letters B

www.elsevier.com/locate/physletb

Nuclear rainbow in the $^{16}O + ^{27}AL$ system: The role of couplings at energies far above the barrier

D. Pereira [a,*], R. Linares [b], J.R.B. Oliveira [a], J. Lubian [b], L.C. Chamon [a], P.R.S. Gomes [b], A. Cunsolo [c], F. Cappuzzello [c,d], M. Cavallaro [c], D. Carbone [c,d], A. Foti [d,e]

[a] *Instituto de Física, Universidade de São Paulo, São Paulo, SP, Brazil*
[b] *Instituto de Física da Universidade Federal Fluminense, Rio de Janeiro, Niterói, RJ, Brazil*
[c] *INFN, Laboratori Nazionali del Sud, I-95125, Catania, Italy*
[d] *Dipartimento di Fisica e Astronomia Università di Catania, I-95125, Catania, Italy*
[e] *INFN – Sez. Catania, via S. Sofia, 64, I-95125, Catania, Italy*

ARTICLE INFO

Article history:
Received 5 December 2011
Received in revised form 9 February 2012
Accepted 12 March 2012
Available online 16 March 2012
Editor: D.F. Geesaman

ABSTRACT

High precision elastic and inelastic angular distributions have been measured for the $^{16}O + ^{27}Al$ system at a beam energy of 100 MeV. The data analysis confirms a rainbow formation as already predicted by parameter-free Coupled Channel calculations. It also helps to reveal the crucial role of inelastic couplings in the rainbow formation for heavier systems even at energies far above the Coulomb barrier. This feature, well known in atomic/molecular scattering, is experimentally studied for the first time in Nuclear Physics.

Rainbow is a very effective mechanism to probe the interaction in atomic/molecular or nuclear scattering. In the first case, examples of pronounced rainbow pattern have been reported since many years [1], and have been explained by inelastic excitation couplings [2]. In nuclear collisions, due to the corresponding strong absorption, appearance of rainbow seems to be restricted to light ion systems [3] consisting of tightly-bound nuclei and having α-cluster structure, like $^{12}C + ^{12}C$, $^{12}C + ^{16}O$, etc. Typically, the optical model (OM) analysis with an adjustable Woods–Saxon shape imaginary potential is the theoretical approach used to account for the rainbow structure in those systems [3,4]. Nevertheless, from OM calculations with realistic potentials [5], no rainbow structure is expected for heavier systems such as $^{16}O + ^{28}Si$, due to the corresponding strong absorption. Recently, a new generation of parameter-free calculations, using the São Paulo Potential (SPP) [6] combined with Coupled Channels (CC) formalism (SPP/CC), has been developed, which take into account dissipative and surface processes in the continuum, like deep-inelastic or break-up reactions. This has been done [7] by the introduction of a parameter-free imaginary potential, which is based on the Glauber model. In the case of systems involving weakly-bound nuclei, OM calculations using this potential approximately reproduce the Continuum Discretized Coupled Channel method (CDCC) results [8]. The interaction $U(R)$ is given by

$$U(R) = V_F(R) e^{-4(\frac{v(R)}{c})^2} (n_r + 0.6i), \quad (1)$$

where $v(R)$ is the local relative velocity, $V_F(R)$ is the double-folding potential, and the exponential term is related to the Pauli non-locality [4]. The normalization parameter n_r assumes the values of $n_r = 1$ or $n_r = 0.6$ in the case of collisions with tightly- or weakly-bound nuclei, respectively. The last case corresponds to a positive polarization from the continuum to bound states which is particularly relevant [3,8,9] in reactions where the projectile break-up is important. This model has been successfully tested [7] for different systems ($^{16}O + ^{27}Al$, ^{58}Ni, ^{60}Ni, $^{58}Ni + ^{124}Sn$, $^{6,7}Li + ^{120}Sn$) in a wide energy range. In particular, for the $^{16}O + ^{27}Al$ system the experimental (fusion, deep-inelastic, quasi-elastic) cross sections, for $E_{LAB}(^{16}O) < 90$ MeV, are in agreement with our theoretical predictions. Moreover, as a non-trivial result, the SPP/CC calculations predict [7] a nuclear rainbow pattern in the angular distribution for the elastic scattering of ^{16}O (at $E_{LAB} = 100$ MeV or higher) on ^{27}Al or ^{58}Ni, which is strongly connected to the coupling with low-lying target excitations. In order to verify the SPP/CC nuclear rainbow prediction, in this Letter we present very precise elastic and inelastic experimental angular distributions for the $^{16}O + ^{27}Al$ system, at a beam energy of 100 MeV far above the Coulomb barrier (29 MeV). The choice of ^{27}Al as target is appropriate to avoid the admixture of the rainbow structure with pronounced cross section oscillations at backward angles, mainly observed in α-cluster nuclei [10] at lower energies. Such a challenging experiment has been performed at the Tandem Van de Graaff accelerator of the INFN–LNS. The use of the large

* Corresponding author.
E-mail address: dpereira@dfn.if.usp.br (D. Pereira).

0370-2693/$ – see front matter
http://dx.doi.org/10.1016/j.physletb.2012.03.032

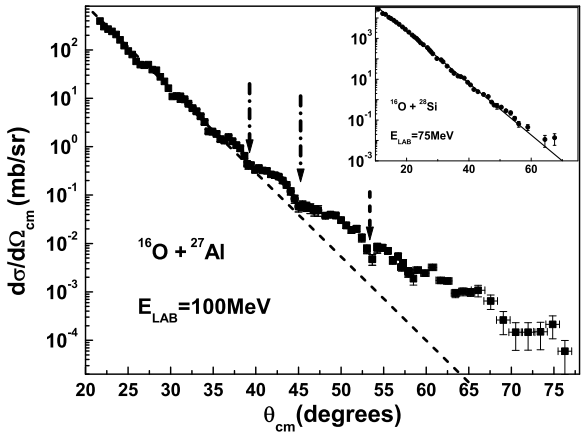

Fig. 1. Experimental elastic angular distribution for $^{16}O + ^{27}Al$ at 100 MeV. The dashed line is a linear fit in the $22° \leqslant \theta_{cm} \leqslant 35°$ angular interval. Airy-like minima are indicated by the arrows. The inset shows elastic angular distribution data for $^{16}O + ^{28}Si$ at 75 MeV, extracted from Ref. [13], together with a linear fit in the $10° \leqslant \theta_{cm} \leqslant 70°$ angular interval (solid line).

acceptance magnetic spectrometer MAGNEX [11] was mandatory for the measurement of very low cross sections (down to hundreds of nb/sr), which also requires negligible background, high energy and angular resolutions and accuracy. A complete description of the experimental procedure has already been published [12].

The experimental elastic angular distribution for the $^{16}O + ^{27}Al$ system at $E_{LAB} = 100$ MeV is shown in Fig. 1. The quality of the data is very high: average angular and energy resolutions (Full Width Half Maximum) of 0.3° and 250 KeV respectively and accuracy of 0.15° have been achieved by the trajectory reconstruction method [11]. In such conditions, a complete separation of the elastic and inelastic events was possible even at backward angles where the corresponding cross sections are comparable [12]. In addition, the background due to elastically scattered particles from the target contaminants (C, O, etc.) and from transfer processes has been eliminated. The straight line in the figure corresponds to a linear least squares fit to the elastic cross sections in the $22° \leqslant \theta_{cm} \leqslant 35°$ angular interval, where the cross section oscillations are connected to the Coulomb–nuclear interference, also known as Fraunhoffer diffraction due to the analogy with the scattering of light. A similar feature can be observed in the elastic scattering of ^{16}O on ^{28}Si at $E_{lab} = 75$ MeV, but in a much larger angular interval $10° \leqslant \theta_{cm} \leqslant 70°$ (see the inset in Fig. 1 – the data was extracted from Ref. [13]). The difference between the two sets of data is clear, without the need of any theoretical analysis. In the present case (^{27}Al), for $\theta > 40°$ the corresponding elastic cross sections systematically deviate from the straight line for increasing backward angles, with sharp oscillations (indicated by the arrows) followed by broad structures, a behavior that characterizes the far-side component of the nuclear rainbow phenomenon (see e.g. [3]). A similar behavior is present in the scattering of $^{16}O + ^{16}O$ at 350 MeV and other well-known cases of nuclear rainbow. While such behavior is not present in the ^{28}Si case at $E_{lab} = 75$ MeV (the largest energy for which there are experimental data in a sufficiently wide angular range up to now), higher energies (at least 6 MeV/nucleon) are critical, according to our calculations, for the formation of the rainbow-like shoulder, both in ^{28}Si and ^{27}Al targets. This can be understood since rainbow scattering requires rather large density overlaps. Also for the $^{16}O + ^{60}Ni$ system, as already mentioned in Ref. [7], the calculations predict clearer rainbow-like patterns as the energy increases, but the experimental data do not reach (by 3–4 orders of magnitude in the relative cross section σ/σ_R) the inflection region, in contrast to the

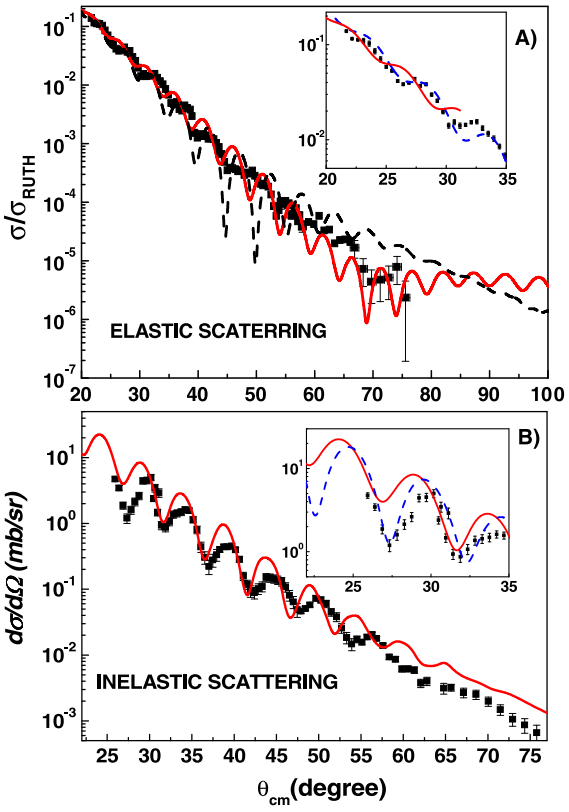

Fig. 2. Experimental angular distributions for the (A) elastic and (B) inelastic (^{27}Al, low-lying states) scattering, as compared with the corresponding theoretical CC predictions (solid lines) and from OM calculations without couplings (dashed line). The insets show expansion regions for which Pauli Blocking (PB) corrected calculations (dashed lines) are also presented (see text).

present case. In addition, significant corrections to the model are anticipated to be necessary for targets much heavier than ^{27}Al, and a similar degree of reliability cannot be achieved.

In Fig. 2, the elastic and inelastic data are compared with the corresponding theoretical SPP/CC predictions (solid lines), obtained using the computer code FRESCO [14]. Taking into account the absence of adjustable parameters, the agreement between the experimental data and the theoretical predictions is good. Despite the deviations with relation to the measured phase of the oscillations, the general trend of both angular distributions is very well described by the calculations up to the inflection region (around 70°). In the CC calculations, we have considered the $1/2^+$, $3/2^+$, $7/2^+$, and $9/2^+$ ^{27}Al low-lying collective states. These states can be described by the weak coupling model, considering a $1d_{5/2}$ proton hole coupled with the 2^+ rotational state of the ^{28}Si core. The deformation length used in the CC calculations was obtained from the ^{28}Si deformation parameter of $\beta = 0.407$ [15] and the ^{27}Al radius of 3.8 fm [9]. This model has been extensively tested with inelastic scattering of proton, deuteron and α on ^{27}Al [16]. The population of the $5/2^+$ state is suppressed since its energy is shifted upwards due to level repulsion from the ^{27}Al ground-state, which has the same spin and parity. No relevant improvement has been achieved in the agreement between the data and the CC calculations by the inclusion of additional target/projectile excited states or transfer processes, although the oscillation phases are rather sensitive to them. For the purpose of comparison, the dashed line in Fig. 2(A) represents the theoretical results obtained with the same optical potential (Eq. (1) with $n_r = 1$) but without couplings. The importance of the inelastic couplings for a better description of the data is clear, particularly in the $55° \leqslant \theta \leqslant 76°$

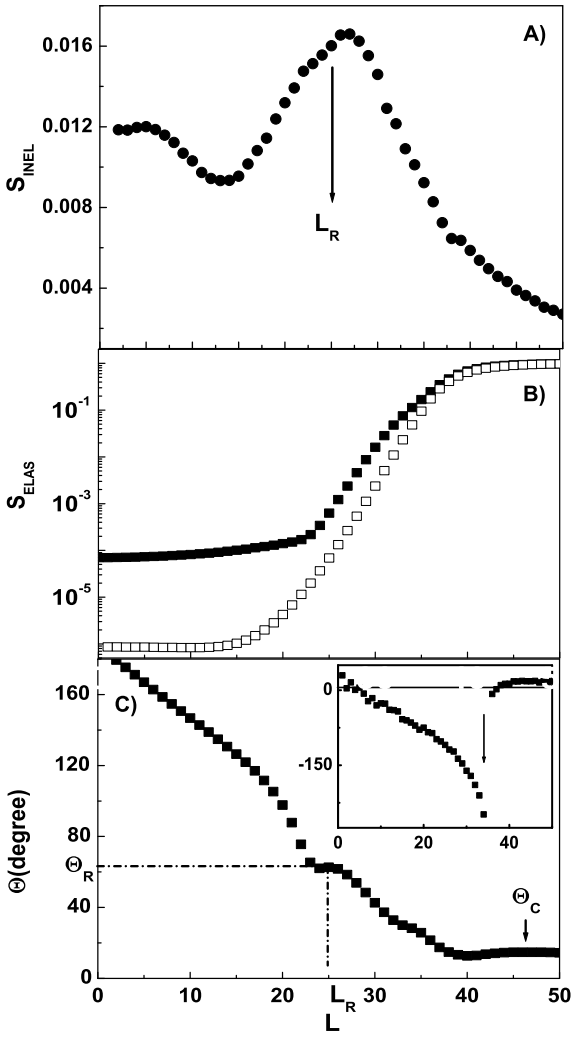

Fig. 3. (A) The nuclear scattering matrix amplitude S for the inelastic state. (B) The elastic S-matrix from two different approaches: CC calculations (closed squares) and OM calculations without couplings (open squares). (C) The corresponding deflection function from CC calculations. The Coulomb and nuclear rainbow angles are indicated in the figure. The inset in (C) shows the classical deflection function where the arrow indicates an orbiting process at $L = 35$.

angular region. The insets of parts (A) and (B) of Fig. 2 are expansions of the respective graphs in which additional calculations are presented with Pauli Blocking (PB) corrections approximately taken into account (dashed lines). PB reduces the imaginary potential by effectively reducing the N–N scattering cross sections. A density dependent reduction factor, according to the parametrized formula of Ref. [17], was applied to the folding procedure for the imaginary potential. This improves the agreement of the oscillation phase with the data in the angular range presented, but fails at higher angles where density overlap is larger and the correction factor becomes overestimated. Although an improvement of this procedure is still necessary, these results show that PB can influence significantly the oscillation phases by changing the shape of the imaginary potential (the real potential is unchanged). PB effects increase with the density of particles and are expected to become more important for heavier systems.

Fig. 3 presents the S-matrices for the inelastic (A) and elastic (B) scattering as a function of the orbital angular momentum. The closed and open squares in (B) were obtained from CC and OM (no couplings) calculations, respectively. The comparison between them, in the strong absorption region of low angular momenta, shows an enhancement of almost two orders of magnitude of the CC results with relation to the OM ones. This behavior is responsible for the possibility of experimental observation of the nuclear rainbow, and resembles the sub-barrier fusion enhancement observed in several systems [18]. On the other hand, at high angular momenta ($L > 35$) the elastic S-matrix from CC is slightly smaller than that from OM. Indeed, the reduction of the CC S-matrix (relative to the OM) at large L values implies a reduction of the CC elastic cross section (relative to the OM) at forward angles ($\theta < 85^\circ$ – see the comparison between CC and OM results in Fig. 2(A)). Furthermore, the enhancement of the CC S-matrix at low L values results in larger cross sections for backward angles ($\theta > 85^\circ$ – see Fig. 2(A)).

From the semi-classical point of view [19], the rainbow is related with the internal branch of the deflection function $\Theta = 2\frac{d\delta}{dL}$, where δ is the total (Coulomb + nuclear) phase-shift. The nuclear rainbow is formed when several values of L provide similar scattering angles about Θ_R, i.e. the function $\Theta(L)$ presents a maximum or a minimum. The rainbow angle divides the scattering angular space into the bright ($\Theta > \Theta_R$) and dark ($\Theta < \Theta_R$) sides. Fig. 3(C) shows the deflection function obtained from the CC phase-shifts. The inset in this figure represents the deflection function obtained from the classical trajectories considering only the real part of the optical potential. For $L = 35$ (arrow in the inset) this classical function provides almost an orbiting process ($\Theta(L = 35) \approx -350^\circ$). The deflection function from CC calculations (including the imaginary part of the potential) is very different than the classical one. The orbiting feature is not present in the CC deflection function since it is strongly absorbed. Usually (for light systems), the nuclear rainbow is associated to a minimum in the negative angle side of the classical deflection function [19]. The present CC deflection function does not present this feature, but is similar to the rainbow case investigated in atom/molecule collisions [20], also associated with inelastic couplings. An oscillation of $\Theta(L)$ (Fig. 3(C)) is observed, with a local maximum at $\Theta_R \approx 63^\circ$ ($L \approx 25$). We therefore infer that the present kind of nuclear rainbow arises from the couplings and consequently is related to a positive polarization for the elastic channel (as discussed below). Indeed, the L value for the rainbow angle above is close, as it should be, to the L value of the maximum observed in the inelastic S-matrix, Fig. 3(A). This important result establishes the origin of the nuclear rainbow in the present studies and, to our knowledge, has not been reported in nuclear physics so far.

Fig. 4 presents an expansion region where the data shows well-defined broad and narrow oscillations that we associate to the Airy (Ai) and Fraunhoffer (F.D) cases, respectively, in analogy with the optical rainbow. Airy oscillations should appear in the situation with very low absorption. The occurrence of the Airy-like oscillations in the present case could be related to some decrease of absorption, probably connected to PB (see above) or other in-medium effects [17]. The solid line in this figure corresponds to the CC cross sections prediction. The usual decomposition of the total scattering amplitude in the near/far components derived from OM calculations without couplings is also presented in Fig. 4. These components serve just as a guide since they are only a rough approximation in relation to those from the exact CC calculations (SPP/CC). Backward and forward cross sections are mainly determined by the contributions of the far-side and near-side components, respectively. The inset in Fig. 4 presents the trivially equivalent polarization potential (TELP) obtained from the CC calculations. It represents an average over the L-dependent polarizations and is responsible for the different patterns of the theoretical angular distributions presented in Fig. 2(A). At the surface ($R > 5$ fm), a region that corresponds to large L values, the real part of the TELP (solid line in the inset of Fig. 4) is slightly

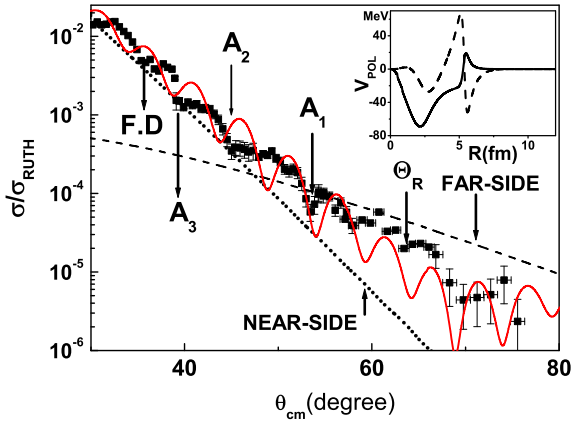

Fig. 4. An expansion of Fig. 2(A) in both axes. The figure shows the experimentally observed Airy-like minima (Ai) and the near/far-side components of the OM calculations (see text). The inset in the figure shows the real (solid line) and imaginary (dashed line) parts of the trivially equivalent polarization potential (TELP) obtained from the CC calculations.

repulsive and the imaginary part (dashed line) is absorptive. At inner distances, low L values, the real part is attractive and the imaginary part is predominantly positive. This behavior is compatible with that of the elastic S-matrix: more absorption (of the CC results relative to the OM ones) at large L values and less absorption at small L values. As already commented, this characteristic results in more flux for the elastic channel at larger angles ($\theta > 85^\circ$) and less flux at smaller angles ($\theta < 85^\circ$). Thus, in the present case, the polarization gives rise to a nuclear rainbow. We mention that, recently, the suppression of the Coulomb rainbow has been reported [21] in the elastic scattering of a system involving a weakly-bound nucleus, $^{11}\mathrm{Be} + {}^{64}\mathrm{Zn}$, at near-barrier energies, that can be understood within a similar analysis of the corresponding TELP.

Summarizing, with the reported high precision elastic and inelastic experimental angular distributions it was possible to characterize the occurrence of the nuclear rainbow scattering in the heavy-ion system $^{16}\mathrm{O} + {}^{27}\mathrm{Al}$, basically as predicted by the SPP/CC calculations. The present findings open new perspectives for further studies to explore the effects of inelastic and reaction couplings in heavy-ion systems at energies far above the barrier and for the development of the models for the imaginary potential.

Acknowledgements

We are indebted for the valuable discussions with Prof. M.S. Hussein and Dr. Rubens Lichtenthäller. This work was partially supported by Istituto Nazionale di Fisica Nucleare (INFN), Fundação de Amparo à Pesquisa do Estado de São Paulo (FAPESP), Fundação de Amparo à Pesquisa do Estado do Rio de Janeiro (FAPERJ), Conselho Nacional de Desenvolvimento Científico e Tecnológico (CNPq) and Coordenação de Aperfeiçoamento de Pessoal de Nível Superior (CAPES).

References

[1] J.R. Lesley, J. Rawluk, Y.B. Fan, Y. Apelblat, M. Keil, J. Chem. Phys. 94 (1991) 4205.
[2] T.W.J. Whiteley, C. Noli, J.N.L. Connor, J. Chem. Phys. A 105 (2001) 2792.
[3] D. Khoa, W. Von Ortezen, H.G. Bohlen, S. Ohkubo, J. Phys. G 34 (2007) 111.
[4] L.C. Chamon, D. Pereira, M.S. Hussein, M.A. Cândido Ribeiro, D. Galetti, Phys. Rev. Lett. 79 (1997) 5218.
[5] M.S. Hussein, K.W. McVoy, Prog. Part. Nucl. Phys. 70 (1983) 136.
[6] L.C. Chamon, et al., Phys. Rev. C 66 (2002) 014610.
[7] D. Pereira, J. Lubian, J.R.B. Oliveira, L.C. Chamon, Phys. Lett. B 670 (2009) 330.
[8] D.P. Souza, et al., Nucl. Phys. A 836 (2010) 1.
[9] J. Lubian, et al., Nucl. Phys. A 791 (2007) 24.
[10] A. Roy, A.D. Frawley, K.W. Kemper, Phys. Rev. C 20 (1979) 2143.
[11] F. Cappuzzello, et al., in: Magnets: Types, Uses and Safety, Nova Publisher Inc., 2011, pp. 1–63;
F. Cappuzzello, et al., Nucl. Instr. Meth. A 638 (2011) 74.
[12] M. Cavallaro, et al., Nucl. Instr. Meth. A 648 (2011) 46.
[13] T. Yamaya, O. Satoh, S.M. Morita, K. Kotajima, K. Hasegawa, T. Shinozuka, M. Fujioka, Phys. Rev. C 37 (1988) 2585.
[14] I.J. Thompson, Comput. Phys. Rep. 7 (1988) 167.
[15] S. Raman, C.W. Nestor Jr., P. Tikkanen, At. Data Nucl. Data Tables 78 (2001) 1.
[16] G.M. Crawley, G.T. Garvey, Phys. Lett. 19 (1965) 228, and references therein.
[17] C.A. Bertulani, C. De Conti, Phys. Rev. C 81 (2010) 064603.
[18] L.R. Gasques, et al., Phys. Rev. C 69 (2004) 034603.
[19] M.P. Pato, M.S. Hussein, Phys. Rep. 189 (1990) 127.
[20] C. Xiahou, J.N.L. Connor, J. Chem. Phys. A 113 (2009) 15298.
[21] N. Keeley, N. Alamanos, K.W. Kemper, K. Rusek, Phys. Rev. C 82 (2010) 034606.